2017 IEEE/RSJ International Conference on Intelligent Robots and Systems (IROS)
September 24–28, 2017, Vancouver, BC, Canada

Design of a Stewart Platform-Inspired Dexterous Hand for 6-DOF Within-Hand Manipulation

Connor M. McCann, *Student Member, IEEE* and Aaron M. Dollar, *Senior Member, IEEE*

***Abstract*—In this paper, we present a novel robotic hand specifically designed for dexterous spatial manipulation. Unlike most other dexterous hand designs that attempt to mimic the kinematic structure of the human hand, the proposed mechanism instead is based on the non-anthropomorphic "hexapod" structure of the Stewart platform parallel manipulator. The hand is composed of a single "grasp" actuator connected via an underactuated differential mechanism to six prismatic actuators arranged into pairs, forming three planar, parallel mechanism fingers that replicate the kinematics of a traditional 6-degree of freedom Stewart platform when grasping an object. This configuration allows for both grasping and accurate manipulation of a range of object sizes/shapes with minimal sensing. We describe the design and fabrication of a prototype hand that incorporates these kinematics and experimentally demonstrate it performing a series of accurate translational and rotational manipulations.**

***Index terms*—Robotics, Hands, Grasping, Manipulation, Mechanisms, Design, Parallel Robots, Stewart Platform**

I. Introduction

While grasping is a crucial "first step" in the majority of object manipulation tasks, manipulating the object after grasping in order to further refine its position/orientation is typically also required [1]. Most research on within-hand manipulation has focused on anthropomorphic architectures that attempt to mimic the form and manipulation capabilities of the human hand by employing a set of multi-phalanx fingers and an opposable thumb [2]–[5]. Some proposed designs even attempt to mimic the tendon routing seen in nature [6].

While the logic behind building anthropomorphic dexterous hands is evident, this strategy may not be optimal for many robotic tasks. Human hands have evolved to cope with a variety of challenges found in nature not relevant to robotic systems, leading to unnecessary complexity in actuation and sensing for many industrial applications [7]. In contrast, in the field of parallel robotics, many non-anthropomorphic parallel manipulator designs have been shown to produce highly dexterous motion with minimal actuation/sensing complexity, such as the common 6-degree of freedom (DOF) "Stewart platform" [8] (which was also proposed earlier by Gough [9] and Cappel [10], all independently). However, up to this point, these mechanisms have not been examined in the context of grasping tasks, such as within-hand manipulation.

Given the similarities that exist between these two classes of systems—robotic hands and parallel manipulators—some mathematical formulations employed for modeling parallel robots have also been adapted for use with hand-object systems [11]. Despite these similarities, however, very little work has been done to merge the actual mechanisms used in these two fields.

Fig. 1. The proposed parallel mechanism hand grasping a softball. All six prismatic actuators (used for 6-DOF manipulation) as well as the single revolute "grasp" actuator in the palm (used to close the hand) are easily visible.

In this paper, we propose a novel parallel mechanism-based hand design that uses three, 2-DOF parallel linkage fingers to achieve dexterous 6-DOF manipulation similar to a Stewart platform (Fig. 1). The hand utilizes an underactuated differential tendon drive to route tension equally from a single "grasp" actuator to the three fingers of the hand. These planar fingers each consist of two linear actuators—as found in a Stewart platform—connected via (3-DOF) spherical joints and (2-DOF) universal joints. The object may be treated as the "platform" of a parallel mechanism, and the contact forces at the fingertips are incorporated into the joint formulation for this parallel manipulator model.

With the exception of some micro-scale manipulator systems [12] and some attempts to integrate parallel mechanisms into the palm of a dexterous hand [13], to the

This work was partially supported by the National Science Foundation grant IIS-1317976.

C. M. McCann and A. M. Dollar are with the Department of Mechanical Engineering and Materials Science, Yale University, New Haven, CT, USA (email: {connor.mccann, aaron.dollar}@yale.edu)

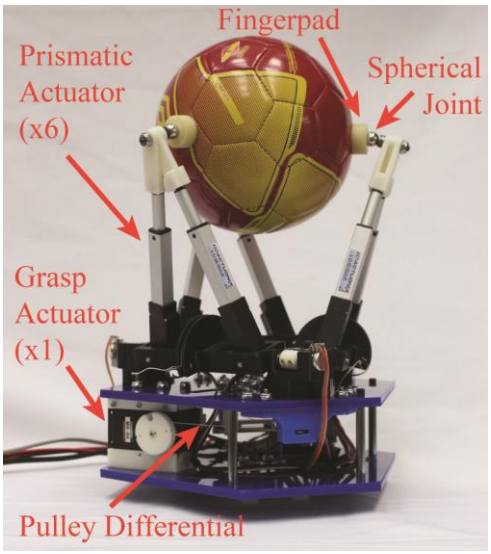

Fig. 2. Overview of the core components of the proposed hand. The grasp actuator exerts a torque about the base of each finger through the pulley differential, closing the fingers on the object until they make contact with the fingerpads. Once contact has been established, the six prismatic actuators are used to manipulate the object.

authors' knowledge, most if not all dexterous multi-fingered hands have relied on serial (often 1-DOF) mechanisms for fingers. Planar parallel linkages (namely, 4-bar linkages) have previously been used for underactuated gripper designs, such as the MARS and SARAH hands. However, in these cases, the parallel mechanism was simply used to provide a differential force transmission between the phalanges of the finger, and did not serve to increase the within-hand manipulation capabilities of the hand [14].

In Section II, we begin with a discussion of the design of the proposed mechanism, and then in Section III derive its kinematics. In Section IV, we present an experimental validation of the design and evaluate its ability to grasp, reposition, and reorient multiple objects. Finally, in Section V, we discuss how the hand may be improved in the future.

II. Mechanism Design

The proposed hand design (Fig. 2) was inspired by a 6-3 Stewart platform. In this configuration, the six universal-prismatic-spherical (UPS) joint legs of the parallel mechanism are joined in pairs. Within each pair, the legs share a spherical joint connection to the platform but have separate universal joints connecting to the base (Fig. 3a). To convert this 6-3 Stewart platform into a hand capable of grasping objects, the spherical joint connection to the platform at the end of each pair of actuators is replaced with a fingerpad mounted on a magnetic ball/socket spherical joint. When the hand grasps an object, the object (coupled to the fingerpads by frictional contacts) corresponds to the platform of the mechanism (Fig. 3b). As a result, each new object—and even different grasps of the same object—will result in a Stewart platform with a new "virtual platform" geometry. To maintain the contact constraints, a torque must be applied at the base of each finger to close the hand inwards on the object and exert a normal force at each contact. The magnitude of the normal force and the coefficient of friction between the fingerpad and the object limit the maximum shear force each fingertip can exert and

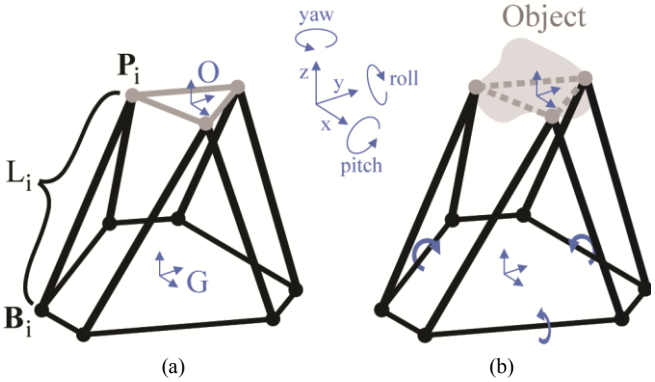

Fig. 3. Schematics of (a) an unaltered 6-3 Stewart platform showing the global and object coordinate frames (G, O) and (b) the proposed Stewart platform-inspired hand with the "virtual platform" shown. The axis conventions put forth here are used throughout the paper.

determine the extent to which the object can be safely manipulated. This inward torque is applied to the fingers by an additional revolute "grasp" actuator in the palm of the hand (Fig. 2) connected through an underactuated differential mechanism to the base of each finger.

A. Finger Design

Fig. 4 illustrates a more detailed view of the linkage employed for each of the three fingers of the hand. Rather than connecting a separate universal joint to the base of each of the two prismatic joints in the finger, as is often done in a conventional Stewart platform, both legs are connected to an intermediary link by revolute joints, forming a triangular planar linkage (Fig. 4b). This, in turn, is connected as a unit to the hand with a second revolute joint. Each finger can be flexed inward toward the object by applying a torque about this intermediary link at the base of the triangle. Additionally, the intermediary link allows a potentiometer to be mounted to this revolute joint at the base of the finger to measure the finger angle. Using the measurements from this potentiometer, the geometry of the virtual platform for each new grasp can be calculated through the finger forward kinematics (presented in Section III), allowing for precise control of the manipulator with differing object shapes. These three potentiometers are the only sensors required by the hand.

To ensure reliable contact between the finger and the object, a concave urethane fingerpad (Fig. 2) was mounted to a magnetic ball/socket joint [15]. Here, an embedded magnet within the cast urethane fingertip couples with a spherical magnet at the end of the finger, forming a 3-DOF ball/socket joint. The polarities of these two magnets initially align the fingertip normal to the plane of the finger before contact is made but allow it to reorient and conform to the surface of the object when contact is established. Due to the way in which this fingertip joint was implemented, a small offset (denoted by **n** in Fig. 4c) was added between the plane of the finger and the center of the spherical joint.

B. Pulley Differential Design

In order to apply equal torque to all three fingers, a 1-to-3 torque-splitting differential was implemented under the palm of the hand. The output of a rotary servo motor (referred to as the grasp actuator) was used to tension a tendon via a pulley

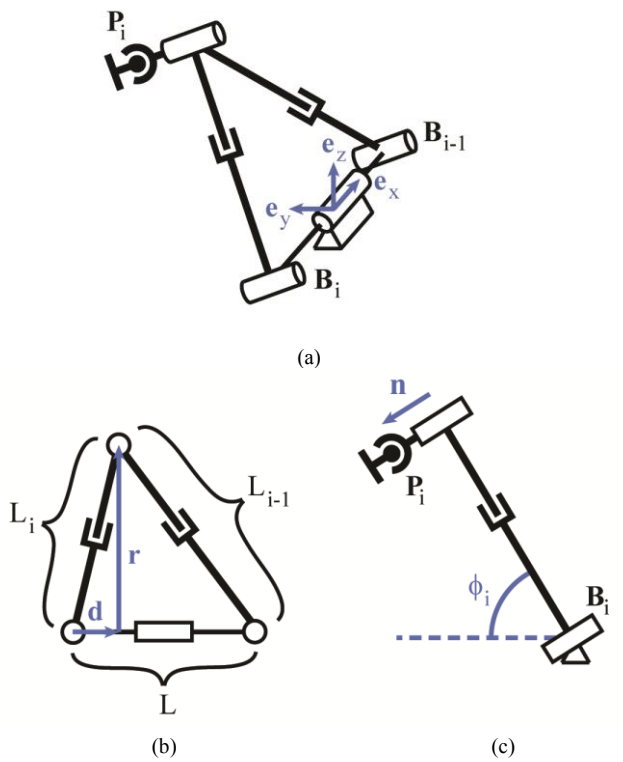

Fig. 4. Finger linkage kinematic configuration. (a) Spatial view showing an additional basis ($\mathbf{e}_x$,$\mathbf{e}_y$,$\mathbf{e}_x$) employed for the forward kinematics derivation in Section III (b) planar linkage view, (c) side view.

drum. This tendon input force was then split twice through a standard pulley tree differential [16] that results in a four-way force split. Since only three outputs were required, one of the four output tendons was terminated on the base of the hand. Each of the three remaining output tendons was terminated on a semi-circular drum on the intermediate link at the base of each finger (visible in Fig. 1 and Fig. 2). A constant inward torque is applied to each finger to maintain the frictional contacts at the fingertips by commanding a constant servo torque. The connection between the object and the fingers can then be modeled as a spherical joint as in a Stewart platform for the subset of the hand's workspace where the fingers do not slip. In this case, the kinematics for the hand-object system simplify to those of a 6-3 Stewart platform with equivalent platform geometry (as determined by the shape of the object being grasped). Thus, the differential within the palm can be ignored for all kinematic considerations when the fingertips do not slip on the object.

III. Hand/Finger Kinematics

In order to control the manipulation performed by the proposed hand, it was necessary to derive its inverse kinematics. Assuming that the fingertips do not slip after making contact with the object, the inverse kinematics of the hand are identical to those for a regular 6-3 Stewart platform. In particular, consider a typical Stewart platform with base and platform joints located at points $\mathbf{B}_i$ and $\mathbf{P}_i$ respectively, as labeled in Fig. 3a (where $i \in \{1\ldots6\}$). For this manipulator to achieve a desired configuration where the object coordinate frame (O) is specified relative to the global frame (G) by a translation vector $\mathbf{T}$ and 3x3 rotation matrix $\mathbf{R}$, the prismatic joints must be set to lengths described by the relation:

$$L_i = \left\| \mathbf{R}\ {}^{O}\mathbf{P}_i + \mathbf{T} - {}^{G}\mathbf{B}_i \right\| \tag{1}$$

where the superscripts O and G refer to vectors expressed in the object and global coordinate frames, respectively [17].

In the proposed hand, however, a correction must be made to account for the offset vector, $\mathbf{n}$, that exists between the plane of the fingers and the spherical fingertip joint (Fig. 4c). This correction can be made as follows:

$$L_i = \sqrt{\left\| \mathbf{R}\ {}^{O}\mathbf{P}_i + \mathbf{T} - {}^{G}\mathbf{B}_i \right\|^2 - N^2} \tag{2}$$

where N is the magnitude of the vector $\mathbf{n}$.

This inverse kinematic mapping, however, is only useful if the geometry of the virtual platform (as specified by the locations of the fingertip spherical joints, $\mathbf{P}_i$) is known. Since the geometry of the virtual platform changes with every grasp, it is necessary to ascertain this geometry for each new grasp before manipulation can begin. This is achieved using the forward kinematics of the fingers in combination with joint angle readings from potentiometers at the base of each finger. If no slipping occurs at the finger contacts, the $\mathbf{P}_i$ vectors will remain constant in the object frame, and therefore need only be found once immediately after a grasp is achieved.

To determine this vector $\mathbf{P}_i$ for a given finger (consisting of legs i and i-1) first the planar motion within the triangle of that finger is examined (Fig. 4b). If the two prismatic joints in the finger are set to lengths L_i and L_{i-1}, respectively, and the base of the triangle has fixed length L, it can be shown from basic geometry that the vectors labeled $\mathbf{d}$ and $\mathbf{r}$ in Fig. 4b have scalar lengths given by:

$$D = (L_i^2 - L_{i-1}^2 + L^2) / (2L) \tag{3}$$

$$R = \sqrt{L_i^2 - D^2} \tag{4}$$

In order to use these offsets to find the spatial position of the point $\mathbf{P}_i$ for each finger, they must be converted into vectors in the global coordinate frame. To do this, a new set of orthogonal unit vectors is introduced at the base of each finger for notational convenience—$\mathbf{e}_x$, $\mathbf{e}_y$, $\mathbf{e}_z$, as shown in Fig. 4a—such that $\mathbf{e}_x$ lies along the axis of the revolute joint at the base of the finger, $\mathbf{e}_y$ lies in the plane of the palm facing toward the center of the hand, and $\mathbf{e}_z$ is normal to the palm. These unit vectors are all expressed in the global frame and are only included to simplify the notation. Using these vectors along with the finger angle ϕ measured relative to the palm using a potentiometer (Fig. 4c), the vectors $\mathbf{d}$, $\mathbf{r}$, and $\mathbf{n}$ can be expressed as:

$$\mathbf{d} = D\ \mathbf{e}_x \tag{5}$$

$$\mathbf{r} = R \cos\phi\ \mathbf{e}_y + R \sin\phi\ \mathbf{e}_z \tag{6}$$

$$\mathbf{n} = N \sin\phi\ \mathbf{e}_y - N \cos\phi\ \mathbf{e}_z \tag{7}$$

Adding all of these vectors in series, along with ${}^{G}\mathbf{B}_i$, the point $\mathbf{P}_i$ can be expressed in the global frame as:

$${}^{G}\mathbf{P}_i = {}^{G}\mathbf{B}_i + \mathbf{d} + \mathbf{r} + \mathbf{n} \tag{8}$$

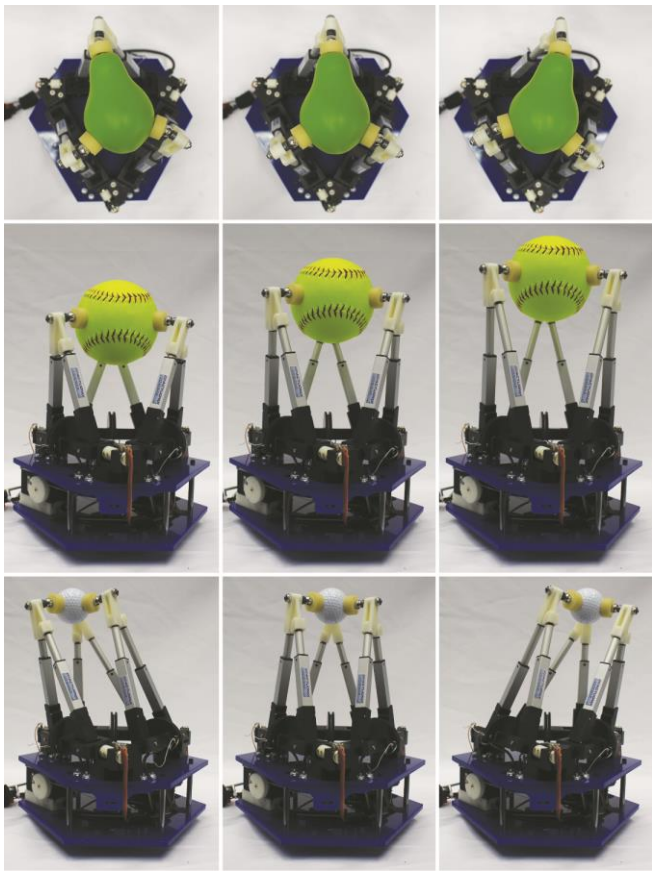

Fig. 5. Examples of manipulations performed with the hand for different objects. *Top:* A plastic pear being rotated ±20 degrees in the yaw direction; *Middle:* A softball being translated ±25 mm in the Z direction; *Bottom:* A golf ball being translated ±50 mm in the X direction.

For this result to be of use in the inverse kinematics expression found in (2), however, $\mathbf{P}_i$ must be expressed relative to the object frame, which is yet to be defined for this particular grasp. To define its location ($\mathbf{T}$) relative to the global frame, its origin is assigned to be coincident with the centroid of the triangle formed by the three ${}^{G}\mathbf{P}_i$ vectors found in (8). Additionally, its orientation is chosen to initially lie parallel to the global frame before manipulation begins. While other conventions are possible to define the object frame, this one proved to be convenient. With the initial location and orientation of the object frame now fully defined, the $\mathbf{P}_i$ vectors can be transformed into this frame, yielding the ${}^{O}\mathbf{P}_i$ vectors needed for use in (2):

$$ {}^{O}\mathbf{P}_i = {}^{G}\mathbf{B}_i - \mathbf{T} \tag{9}$$

In summary, after a given grasp has been achieved, the finger forward kinematics defined in (8) are used to locate the three spherical joints defining the virtual platform in the global frame (${}^{G}\mathbf{P}_i$). The centroid of these points ($\mathbf{T}$) is used to define the object coordinate frame. Finally, the spherical joint coordinates are transformed using (9) into this new object frame (yielding ${}^{O}\mathbf{P}_i$) for use in the hand-object inverse kinematics, as defined in (2). Assuming that no major slipping occurs throughout the manipulation, these spherical joint positions can be taken to be constant for the remainder of the grasp.

IV. Experimental Demonstration

In order to experimentally validate the proposed design, a proof-of-concept prototype was constructed. To actuate the pulley differential to close the hand, a Robotis Dynamixel MX-64 servo motor was used in torque-control mode as the grasp actuator. Additionally, six Actuonix L-12 50-millimeter linear servo motors were used for the prismatic joints, imposing size constraints on the system that resulted in a hand with a base diameter of 152 millimeters. While a formal design optimization has not yet been performed, for a conventional Stewart platform the workspace is maximized when the platform and base have equal diameters [18]. Given that our magnetic spherical joint implementation resulted in an offset vector $\mathbf{n}$ with a length of 16 millimeters, this suggests that the optimal object size for the constructed hand would be approximately 120 millimeters in diameter. This hypothesis is revisited in the results section.

A. Experimental Procedure

The prototype that was constructed successfully performed significant translational and rotational motions for multiple objects (see Fig. 5 and the supplementary video attachment). To characterize the extent of its manipulation capabilities, a set of experiments were performed in which objects were manipulated along linear trajectories in each of the six principle degrees of freedom (x, y, and z translation as well as roll, pitch, and yaw rotation, as defined in Fig. 3) and the maximum range of travel achieved in each direction was recorded. To consistently sample the workspace in each of these six directions, all motions were initiated from the center of the workspace with the linear actuators extended to 50% of their maximum travel. These motions represent only a subset of the hand's reachable workspace and do not capture the coupling between translational and rotational travel limits throughout the mechanism's workspace. That said, they still provide an experimental metric with which to compare the hand's performance across different objects. In future work, after the hand mechanism geometry has been formally optimized, the authors intend to perform more complete workspace analyses/experiments. Four objects were tested: a golf ball, softball, and miniature soccer ball to cover a large size range, as well as a plastic pear oriented along the Y-axis as shown in Fig. 5 to demonstrate the hand's ability to manipulate some less regular geometries.

To define the travel limits of the hand in any particular axis, only cases where neither rolling nor slipping occurred were classified as successes, as both of these behaviors violate the assumption that the virtual platform does not change in shape throughout a motion. Thus, the values recorded represent a conservative estimate of the hand's workspace limits, given that improved modeling and further hardware design iteration might help mitigate these issues.

During any given trial, the object being studied was grasped by the hand and manipulated to a target position along one of the six trajectories using the hand inverse kinematics. This target position was gradually incremented until failure occurred or an actuator travel limit was reached. Between each manipulation, the object was released and re-grasped to ensure that it did not slip over time in any way that might affect the results in an uncontrolled manner. For consistency, any case in which rolling resulted in the fingertip separating from the

Fig. 6. Example of a fingertip rolling failure that was sometimes encountered near the limits of the workspace for certain manipulations. In these cases the object would roll on the fingertip rather than the spherical joint reconfiguring. Separation of greater than 4 mm was classified as a failure.

object surface by more than 4 mm (as shown in Fig. 6) was considered a failure.

B. Experimental Results and Discussion

The results of these manipulation trials are presented in Fig. 7. Here, the maximum and minimum successful manipulations are shown for each of the six axes of interest. In all of the translational axes, consistent manipulation of ±25 mm was achieved. For certain axis/object combinations, this range was as large as ±55 mm (as in the case of the golf ball and pear in the X direction). Likewise, for rotation, all objects were able to achieve ±10 degrees of motion in all axes, with some objects being able to be manipulated considerably further (up to ±27 degrees for the golf ball in the pitch direction).

Moreover, the fact that the pear could be manipulated to a similar extent as the other objects (and in some cases further) demonstrates that the hand is not limited to spherical object geometries. For highly irregular object geometries or ones that did not align well with the axes of the three fingers, the hand was not consistently able to achieve a stable grasp, and thus, manipulation data could not be collected. In future iterations of the hand, the mechanism design will be optimized to allow a wider range of objects to be grasped.

A few distinct failure modes for the grasps were observed and recorded. For manipulations near the center of the workspace, no failure was observed, and the fingertips remained flush to the object surface throughout the motion without noticeable sliding or rolling. These are the cases reported in Fig. 7. Moving further from the center of the workspace, rolling was often observed where one or more of the concave fingertips would "peel" away from the object, resulting in a point contact on the edge of the fingertip (an extreme example of this type of failure is shown in Fig. 6). This motion effectively alters the virtual platform geometry mid-manipulation, leading to inaccuracies in the assumption that the ${}^{O}\mathbf{P}_i$ vectors do not change throughout the motion. That said, this rolling motion appeared to be reversible, as the object would return to its original configuration when the linear actuators were restored to their initial state. Therefore, with improved modeling of the contact forces at the fingertips, as well as alterations in the fingertip/magnetic spherical joint designs, this type of error could be reduced. In particular, the magnets used on this prototype to mount the fingerpads to the fingers were very powerful, resulting in a strong restoring force that often prevented the fingertip from rotating freely. In future iterations of the hand, this magnetic force could be reduced to minimize rolling.

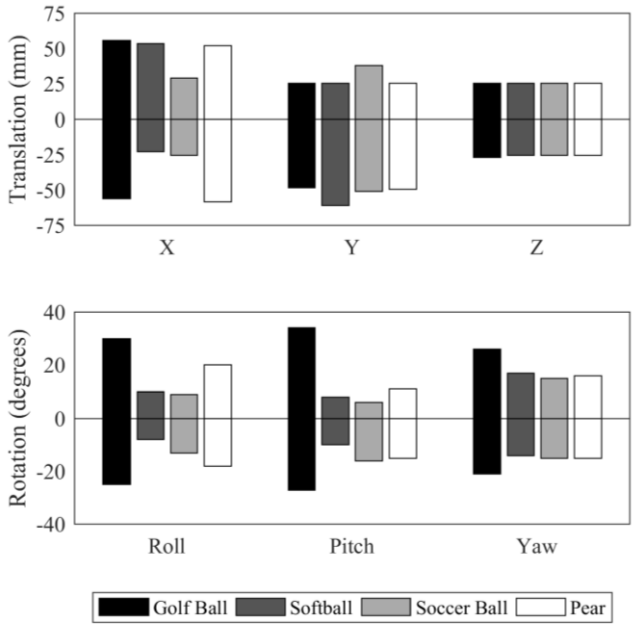

Fig. 7. Maximum and minimum travel distances/angles recorded for each of the six principle axes across four objects.

As the object neared the edge of the stable workspace, a sliding failure mode was also sometimes observed where the fingertips would slip in a non-reversible manner along the object surface. In this case, there would be no way to predict the pose of the object after the manipulation, indicating a significant loss in controllability. Sliding failures were relatively rare, only occurring consistently in the Y direction, about which the hand is asymmetric and the force from one finger would push the object between the other two, causing a sliding motion. Typically, sliding failures resulted in the ejection of the object from the hand, representing a complete failure of the grasp. Ejections were also observed for some extreme rotational motions where the rolling became significant enough to fully separate the fingertip from the object surface. Despite the presence of these failure modes for some extreme motions, most of the trajectories tested were able to continue until an actuator travel limit was encountered, and the object would never be ejected from the grasp.

A few unexpected results can be observed in Fig. 7. As stated previously, the workspace of a standard Stewart platform is maximized when the platform and base have equal diameters. If this same trend applied to the proposed hand mechanism, one would expect the softball to have the largest range of manipulation, as it is the closest to the 120 mm diameter required to make this condition true. That said, this result was not observed. Instead, the smallest object (the golf ball) possessed the largest workspace. With further modeling of the contact forces exerted on an object, it may be possible to explain this behavior and further optimize the hand to achieve similar dexterity for larger objects.

Additionally, it is worth noting that many of the manipulation limits presented in Fig. 7 (such as those in the Z direction for all objects) occurred when a travel limit in one of

the prismatic actuators was encountered, rather than corresponding to a grasp failure. This further indicates the need to optimize the mechanism geometry to maximize the usable workspace of the hand. For the trials that failed before an actuator limit was reached, the failure mode was almost always due to excessive rolling. As described previously, this issue can be corrected by altering the fingertip design in future iterations.

V. Conclusions and Future Work

In this paper, we presented a novel parallel mechanism hand design inspired by a 6-3 Stewart platform. This hand uses three 2-DOF fingers consisting of two prismatic joints to achieve dexterous, 6-DOF motion for a variety of objects, with a seventh "grasp" actuator serving to close the hand. A prototype of the hand was constructed and used to demonstrate the efficacy of the design. With minimal sensing, objects of previously unknown size and shape were able to be manipulated in 6-DOF. While the hand was not able to achieve stable grasps for highly irregular objects, it was able to manipulate non-spherical objects such as a pear. Future versions of the hand will be refined further to grasp more irregular object geometries.

The behavior of the hand was experimentally explored for four objects and the extent of possible reconfiguration in each degree of freedom was characterized. In all translational directions, reconfiguration of ±25 mm was achieved, and in all rotational directions, ±10 degrees of reorientation were possible. Additionally, significantly larger motions were observed for certain object sizes in some directions. The primary factors limiting the workspace of the manipulator were actuator travel limits and fingertip rolling failures that reduced the accuracy of the manipulation near the edge of the workspace.

In future work, the contact forces at the fingertips will be modeled, resulting in improved control of the hand to account for issues such as rolling. Using this model, it will be possible to optimize the geometry of the hand to achieve the largest dexterous workspace possible for a wider variety of object geometries. Additionally, improvements in the fingertip design may also reduce rolling, thereby increasing the reachable workspace volume. Overall, the authors believe that parallel mechanism-based hands provide an exciting, new approach to dexterous in-hand manipulation that warrants further exploration.

Acknowledgment

The authors would like to thank Spencer Backus and Glenn Weston-Murphy for their feedback and contributions throughout the development process.

References

[1] R. Ma and A. Dollar, "On dexterity and dexterous manipulation," in *International Conference on Advanced Robotics (ICAR)*, 2011.

[2] J. K. Salisbury, "Design and Control of an Articulated Hand," in *Proceedings of the International Symposium on Design and Synthesis*, 1984.

[3] M. Grebenstein *et al.*, "The DLR hand arm system," in *International Conference on Robotics and Automation (ICRA)*, pp. 3175–3182, 2011.

[4] H. Kawasaki, T. Komatsu, and K. Uchiyama, "Dexterous anthropomorphic robot hand with distributed tactile sensor: Gifu hand II," *IEEE/ASME Trans. Mechatronics*, vol. 7, no. 3, pp. 296–303, 2002.

[5] C. S. Lovchik and M. A. Diftler, "The Robonaut hand: a dexterous robot hand for space," in *International Conference on Robotics and Automation (ICRA)*, vol. 2, pp. 907–912, 1999.

[6] Z. Xu and E. Todorov, "Design of a highly biomimetic anthropomorphic robotic hand towards artificial limb regeneration," in *International Conference on Robotics and Automation (ICRA)*, pp. 3485–3492, 2016.

[7] A. Bicchi, "Hands for dexterous manipulation and robust grasping: a difficult road toward simplicity," *IEEE Trans. Robot. Autom.*, vol. 16, no. 6, pp. 652–662, 2000.

[8] D. Stewart, "A platform with six degrees of freedom," *Proc. Inst. Mech. Eng. 1847-1982*, vol. 180, no. 1965, pp. 371–386, 1965.

[9] V. E. Gough and S. G. Whitehall, "Universal Tyre Test Machine," in *Proceedings of the FISITA Ninth International Technical Congress*, pp. 117–137, 1962.

[10] K. L. Cappel, "Motion Simulator," US3295224, 1967.

[11] J. Borràs and A. M. Dollar, "Analyzing dexterous hands using a parallel robots framework," *Auton. Robots*, vol. 36, no. 1, pp. 169–180, 2014.

[12] T. Tanikawa, T. Arai, and T. Masuda, "Development of micro manipulation system with two-finger micro hand," in *International Conference on Intelligent Robots and Systems (IROS)*, vol. 2, pp. 850–855, 1999.

[13] L. Cui and J. S. Dai, "Posture, Workspace, and Manipulability of the Metamorphic Multifingered Hand With an Articulated Palm," *J. Mech. Robot.*, vol. 3, no. 2, 2011.

[14] T. Laliberté and C. Gosselin, "Actuation system for highly underactuated gripping mechanism," US6505870 B1, 2000.

[15] R. R. Ma, N. Rojas, and A. M. Dollar, "Spherical Hands: Toward Underactuated, In-Hand Manipulation Invariant to Object Size and Grasp Location," *J. Mech. Robot.*, vol. 8, no. 6, 2016.

[16] L. Birglen, T. Laliberté, and C. Gosselin, *Underactuated Robotic Hands*, vol. 40. Berlin, Heidelberg: Springer Berlin Heidelberg, 2008.

[17] B. Dasgupta and T. S. Mruthyunjaya, "Stewart platform manipulator: A review," *Mech. Mach. Theory*, vol. 35, no. 1, pp. 15–40, 2000.

[18] O. Masory and J. Wang, "Workspace evaluation of Stewart platforms," *Adv. Robot.*, vol. 9, no. 4, pp. 443–461, 1994.